International Journal of Physics and Applications

E-ISSN: 2664-7583
P-ISSN: 2664-7575
IJOS 2022; 4(1): 23-34

www.physicsjournal.in
Received: 15-01-2022
Accepted: 18-02-2022

Shashank Sharma
Department of Physics,
Dr. CV Raman University,
Kargi Road, Kota, Bilaspur,
Chhattisgarh, India

Sanjay Kumar Dubey
Department of Physics,
Dr. Radha Bai, Government.
Navin Girls College, Raipur,
Chhattisgarh, India

Corresponding Author:
Shashank Sharma
Department of Physics,
Dr. CV Raman University,
Kargi Road, Kota, Bilaspur,
Chhattisgarh, India

Structural, optical & thermal characteristics of $M_2MgSi_2O_7$ (M = Ca) Nano phosphor prepared via low temperature combustion synthesis technique

Shashank Sharma and Sanjay Kumar Dubey

Abstract
$Ca_2MgSi_2O_7$ (CMS) nano phosphor was prepared by Combustion Synthesis technique. XRD, SEM, EDX, FTIR, PL spectra and CIE Color Chromaticity Co-ordinate Diagram as well as TL characteristics have briefly investigated. The phase formation of synthesized sample was displayed $P\bar{4}2_1m$ space group with akermanite type tetragonal crystal structure. This crystal structure creates a layered compound. It belongs to mellite group. The average crystallite size (D) is calculated as 31.91nm and lattice strain as 0.25nm. The chemical composition of the synthesized phosphor was well clarified with the help of EDX spectroscopy. The actual phase formation and functional groups identification of this phosphor have been shown with the help of FTIR spectroscopy. In Photoluminescence (PL) characteristics such as Excitation and Emission spectra were also investigated. The phosphor displayed single emission peak at 472nm. The CIE chromaticity coordinates have calculated as [X = 0.2445, Y = 0.2679] respectively. The CIE diagram has shown that this phosphor approached to blue light luminescent color region. In Thermo luminescence (TL) study, the sample UV exposed for 15 min gives optimum TL intensity and single TL glow curve peak was allocated at 152.43°C temperature respectively, and this peak position remains constant with 15min UV irradiation time.

Keywords: $Ca_2MgSi_2O_7$ (CMS), mellite, combustion synthesis, akermanite, x-ray diffraction pattern (XRD)

Introduction
In modern times, luminescence has made an amazing contribution to the field of material science. Solid-state lighting (SSL) and Light Emitting Applications (LEDs) are in great demand. Thus, the white light emitting diodes (WLEDs) have emerged as a superior attraction for solid-state lighting (SSL) source applications. The availability of different varieties of colorful LEDs has added to the lighting market and industries which is continuously growing. Observationally, it turns out that the main reason behind all this is the better performance of the host materials. These host materials form a basic pillar for the doping process. The best long persistent phosphor ever discovered in the history of luminescence is $SrAl_2O_4:Eu^{2+}$, Dy^{3+}, whose long after glow persistency is ~20 hours [Matsuzawa *et al.*(1996)] [1]. For the past few years, material scientists and researchers have been developing better host materials. So that, the better long after glow phosphor can be prepared by doping process of different types of rare earth ions. In the recent few years, the demand for energy is increasing continuously in our present society i.e. energy is the future demand for all of us. Additionally, there is need to focus our attention on important global issues such as saving energy and protecting the environment. With the aim of overcoming the problem of energy shortage and environmental pollution, the ongoing process of actively researching and developing various types of white light emission phosphors. The phosphors converted (pc) solid-state lighting (SSL) sources have been conferred exclusive properties such as long lifetime, energy saving, high efficiency and ecofriendly etc. In this way, we can say that the better implementation of host materials make the doping process more accessible and efficient. In general, it would be fair to say that the host material plays a pivotal role in the discovery of new phosphors. Silicate based phosphors have been widely investigated due to consisting of their exclusive properties, such as rigid crystal structure, water resistance, high brightness, high thermal, physical and chemical stabilities, low-cost and strong absorption in the near-UV (Ultra-violet) region [Tam *et al.* (2014) [2], Tingqiao *et al.* (2016) [3], Yuan *et al.* (2012) [14], Ju *et al.* (2014) [5], Liu *et al.*

(2016)] [6].

Rare-earth doped silicate phosphors have displayed sufficient practical applications such as optical display devices, detector systems, solar cell, scintillates, lasers of phosphors making and many other varieties of light emitting diodes (LEDs) [Tshabalala *et al*. (2016)] [7].

Mellite are a large crystal-structured group of compounds whose represented by means of usual structure representation [i.e. $M_2X^1Y_2{}^2O_7$, where M= Ba (Barium), Sr (Strontium), Ca (Calcium); X^1 = Mg (Magnesium), Zn (Zinc), Cu (Copper), Mn (Manganese), Co (Cobalt); Y^2 = Ge (Germanium), Si (Silicon)]. As an optical material, this crystal structure is widely studied [Sharma *et al*. (2021)] [9]. Akermanite, which is belongs to the family of soro-silicates. The di calcium magnesium di silicate is also called as a host for long-lasting phosphors, generally activated with various RE ions, such as (Eu^{2+}, Nd^{3+}, Dy^{3+} or Mn^{2+}). This CMS phosphor has been extensively discussed in biological and medical areas of applications [Karacaoglu *et al*. (2015)] [10]. Silicate with akermanite structure may be a possible and attractive bio ceramics for tissue engineering applications [Bhatkar *et al*. (2011)] [8]. Akermanite (CMS) crystal structure exhibits superior biocompatibility and bioactivity features. For this reason, they are also identified as probable candidates for bone material [Sharma *et al*. (2021)] [9]. Our present research study is based on a brief investigation including XRD, FTIR, SEM, EDX, PL, CIE Diagram and TL characteristics of sintered CMS nano- phosphor samples.

Experimental analysis

Sample Preparation

The combustion synthesis method have been developed in an facile, fast, versatile, cheaper (i.e. low-cost) and more efficient pathway with a behavioral approach to rapidly producing of a extensive category of catalysts, ceramics and nano-sized luminescent-materials (i.e. phosphors) as well as oxides [Patil *et al*. (2002) [12], Aruna *et al*. (2008) [13], Patil *et al*. (2008)] [14]. Commonly, inorganic phosphor samples are sinteredvia anun-doped host-crystal lattice matrix as well as intentionally compiled by a very slight amount of impurities (i.e. catalyst). When deciding on a host phosphor material and appropriate concentration of the catalyst. So at that time some special things need to be taken into consideration such as its physical characteristics such as surface field, crystallinity, phase accuracy and proper & prescribed distribution of catalyst in the host crystal lattice play an exceedingly relevant contribution in regularizing luminescence properties [Muresan *et al*. (2011)] [15]. In our present investigation, we have applied combustion synthesis technique for sample preparation [Fig: 1]. This process itself is the best material synthesization technique. Basically, the purpose of preparing nano phosphors (i.e. luminescent material) and other type of ceramic products have been attracted more and more attention from researchers and material scientists. That is, gave birth to a deep interest in them. Simultaneously, multi-component, fine particle size, crystalline and homogenous materials were synthesized at relatively very low temperature and short period of time duration [Kim *et al*. (2003)] [16]. All precursor materials have been used as starting materials such as Ca $(NO_3)_2$ (Analytical-Reagent Grade), $SiO_2 * H_2O$ (Analytical-Reagent Grade), NH_2CONH_2 (Urea) (Analytical-Reagent Grade), Mg $(NO_3)_2$ (Analytical- Reagent Grade), and H_3BO_3 (Boric Acid) (Analytical Reagent Grade) with (99.99%) purity in our experiment. The oxidizer and fuel need to be used in very small quantities. In present research work, NH_2CONH_2 (urea) is utilized as a combustion fuel and H_3BO_3 (boric acid) is utilized as an oxidizer (i.e. flux). It is more essential to note that the entire precursor reagents with convenient molar-ratio should be solubilizing in a very slight quantity of CH_3COCH_3 (Acetone) (Analytical Reagent Grade) homogeneously to obtain a very clear solution. The measured amount of each metal nitrates, flux (i.e. oxidizer) and fuel were grinded with the help of 5" agate mortar and pestle for fifteen minute to turn into a thick-paste solution. The resulting solution is placed into a cylindrical crucible (i.e. silica) with a relatively large volume as well as transferred into pre-maintained [i.e. at 650°C temperature] muffle furnace. In about 5min, the overall combustion process has been finished. It is clear from observation that the mixture-solution enters in thermal-dehydration process within a few minutes. Basically, products with gaseous nature are obtained during this process, in which silicates are yielded and ignited to produce a self-propagating flame. As a result, the process of self-propagating ends after a few seconds. The crucible is then taken out of the muffle furnace and kept in an open space to cool down. As soon as the cooling process is over, as a result we get fluffy form of the phosphor sample. Then, it is finely crushed with the help of agate mortar and pestle. Subsequently, the obtained powder material was post-annealed at 950°C temperature for 1 hour. At 5°C per minute, the heating as well as cooling rates were set of the muffle furnace. After subsequent grinding, the final sintered white powder sample was achieved which results its conversion into superfine powder sample. In air-tight bottle, the resulting powder sample was restored for further studies. The chemical process is given as:

$$Ca\ (NO_3)_2 + Mg\ (NO_3)_2 + SiO_2 * H_2O + NH_2CONH_2 + H_3BO_3 \rightarrow Ca_2MgSi_2O_7 + H_2\ O\ (\uparrow) + CO_2\ (\uparrow) + N_2\ (\uparrow) \quad (1)$$

Sample Characterization

For phase structure determination, an X-ray diffraction (XRD) pattern of sintered powder material sample was investigated using Bruker D8 advance X-ray powder diffract to meter with Cu-Kα radiation having 1.5405 Å wavelengths (i.e. at 40 kV and 40 mA). The surface morphology Images of the material sample was analyzed with the help of Scanning Electron Microscope (Model: ZEISS EVO 18). FTIR spectra were also recorded with the help of Bruker-Alpha FTIR spectrometer. An EDX spectrum was utilized for the elemental composition analysis. For identifying the absorption of functional group region (4000 to 1400 cm^{-1}) and the finger-print region (1400 to 400 cm^{-1}) and vibrational features of sintered sample through adding with potassium bromide (KBr) powder sample [Analytical-Reagent Grade] with pallet preparation. In PL study, excitation and emission spectral data were carried out with the help of SHIMADZU, RF-5301 PC spectro-fluoro photometer whose confers refined excitation and emission spectral data and curves in the range between[200-400nm and 475-700nm] respectively. CIE chromaticity diagram was recorded with the help of GO-CIE (1931) software. TL glow curves were plotted between emitted TL intensity and the temperature of the sample were recorded using routine TL set-up Nucleonix TLD Reader (TL 1009I) with constant heating rate 5°Cs^{-1}.In each measurement, 6mg of the phosphor was used. All measurements were recorded at the room temperature.

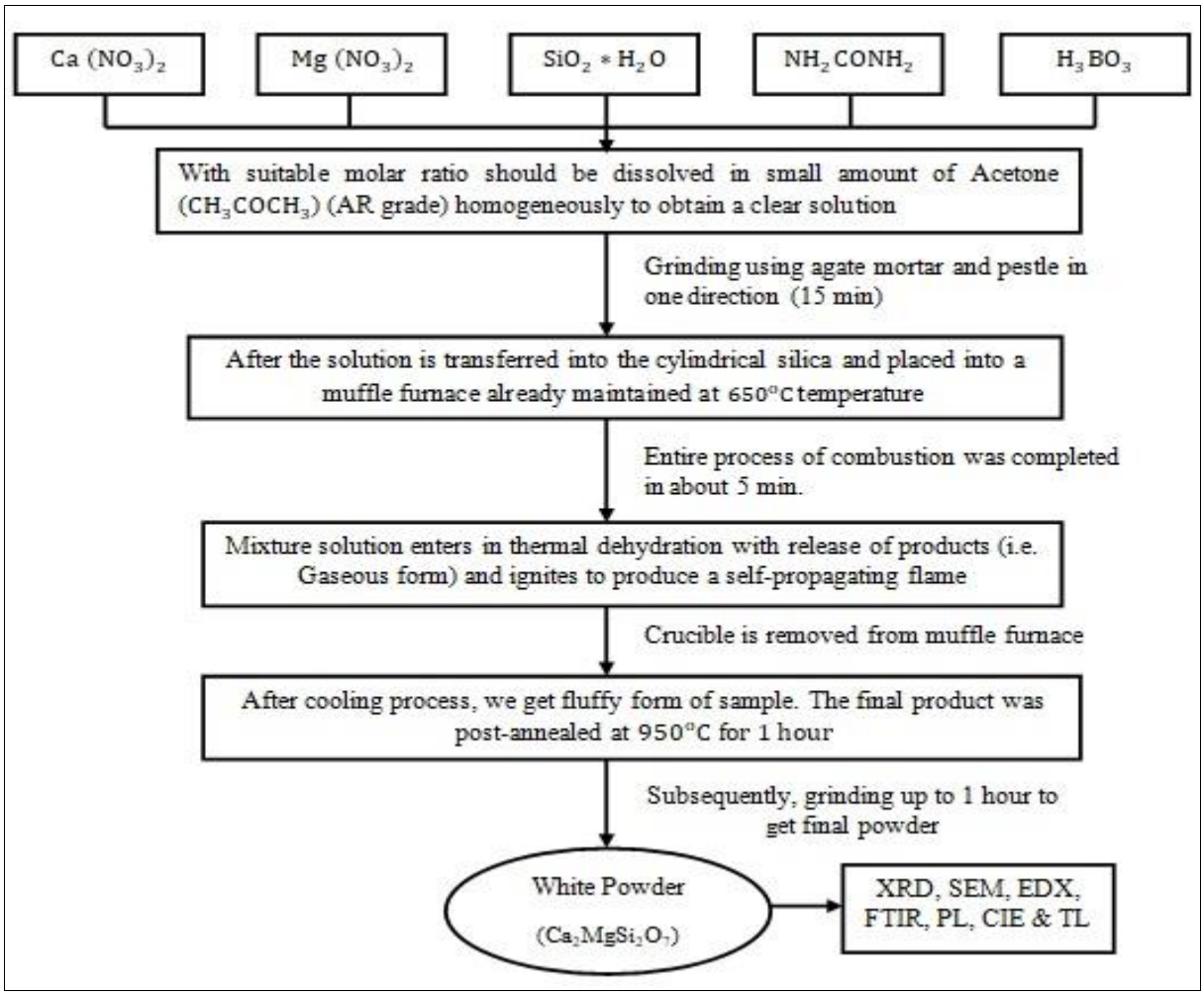

Fig 1: Flow chart of sample synthesization process

Results and Discussion

X-Ray diffraction (XRD)

XRD has a unique place of its own as an important technical technique with multilateral and non-destructive features which is better utilized for the purpose of revealing elaborated information in terms of chemical composition and crystallographic phase structure of synthetic (i.e. inartificial) and fabricated material samples. It would be fair to say that XRD is the most important experimental technique ever developed by which the crystals phase identification of any phosphor sample is performed very precisely. It can also be utilized for successful implementation of lattice constants and geometry, imperfections (i.e. defects), preferred orientation of poly-crystals, recognition of unfamiliar samples, configuration examination of single crystals, strains such as various related problems etc. Specially, used in a variety of applications (i.e. grain shape fixation, degree of crystallinity in mixture sample of crystalline and non- crystalline matters and phase recognizance) [Friedbacher *et al*. (2011) [17], Lyman *et al*. (1993)] [18]. XRD pattern of sintered $Ca_2MgSi_2O_7$ phosphor sample has been shown in Fig. 4. To observe the phase structure, XRD (X-ray Diffraction) data has been carried out in the range between ($10^0 \backslash 2\theta \backslash 80^0$). The XRD diffraction peak positions are well examined with the standard (JCPDS# 77-1149) [JCPDS PDF File] are displayed in Fig: 4. The standard $Ca_2MgSi_2O_7$ CMS crystal formation, crystal lattice parameters and cell-volume are examined with the help of AMCSD 0008032 [American Mineralogist Crystal Structure Data-Base-Code]. XRD diffraction peaks were assigned at (16.10), (21.14), (22.37), (23.84), (25.13), (29.19), (31.24), (32.75), (35.34), (36.12), (38.64), (44.07), (46.16), (48.47), (51.63), (61.94), (64.94), (67.25) corresponding to (110), (101), (200), (111), (210), (201), (211), (220), (002), (310), (102), (212), (410), [(222), (330)], [(310), (312)], (332), (223) and (521) planes respectively. When the diffraction peaks obtained from XRD were closely observed. Then some special results emerged that the phase structure of synthesized phosphor, which relates to akermanite type tetragonal crystal structure with a $P\bar{4}2_1m$ (i.e. 113 space number and D_2d space group) space group and the cell parameters were examined to be a = b = 7.8071 Å, c = 4.9821 Å with $\alpha = \beta = \gamma = 90°$ [Sharma *et al*. (2021)] [11]. Debye–Scherrer equation is demonstrated as: $D = K\lambda/\beta Cos\theta$, where K indicates the Scherrer constant (i.e. 0.94), λ indicates wavelength (i.e. incident X-ray beam), β indicates the FWHM of the peaks and θ indicates the analogue Bragg diffraction angle [Feitosa *et al*. (2004) [21], Ubale *et al*. (2007)] [22]. D (i.e. average crystallite size) is calculated as 31.91 nm.

The average crystalline size and strain was calculated from the width of prominent peak at (2θ) ~ 31.24 with respect to XRD (211) plane. The strain [Uniform Deformation Model (UDM)] was determined with the help of the following mathematical representation: $\varepsilon=\beta/4\tan\theta$ [Sharma *et al*. (2021)]. The sintered CMS sample was obtained as an optically translucent (i.e. semi-transparent) and white (i.e. colorless) powder. The lattice parameters of sintered phosphor materials have shown in Table no. 1.

Table 1: Various Parameters of synthesized phosphor

No.	Parameters	$Ca_2MgSi_2O_7$ Phosphor
1.	Crystal Structure	Tetragonal/Akermanite
2.	Space Group	$P\bar{4}2_1m$
3.	Lattice parameters	a = b = 7.8071 Å, c = 4.9821 Å& $\alpha = \beta = \gamma = 90^{\circ}$
4.	Crystallite size D (nm)	31.91 nm
5.	2θ (Deg)	31.24
6.	Cell Volume (V)	303.663 $Å^3$
7.	Crystal plane spacing d (Å)	2.8630 Å
8.	Strain	0.25nm

Crystal Structure

According to the crystal structure of $Ca_2MgSi_2O_7$ phosphor, four independent cation sites, namely, Ca_1^{2+}, Ca_2^{2+}, Mg, and Sexist in the crystal lattice. Ca_1^{2+} is coordinated by eight oxygen atoms, Ca_2^{2+} is coordinated by six oxygen atoms and both Mg^{2+} and Si^{4+} cations occupy in the tetrahedral sites. All of the calcium atoms are located in the channel and coordinated by oxygen atoms in both the structures (Figure: 2 & 3) [Yao *et al*. (1998) [23], Lin *et al*. (1999) [24], Chaplot *et al*. (2000) [25], Jung *et al*. (2009) [26], Yonesaki *et al*. (2009)] [27]. The physical, chemical and crystallographic features of this standard phosphor sample have been displayed in Table no. 2 as follows.

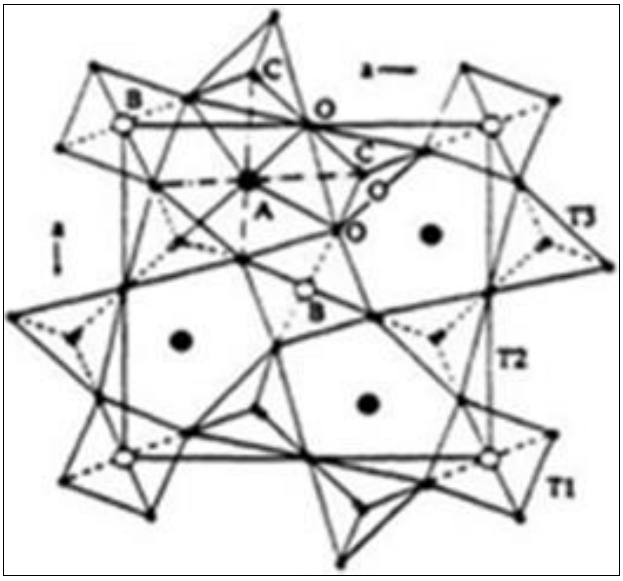

Fig 2: Akermanite crystal structure projected on (001) plane

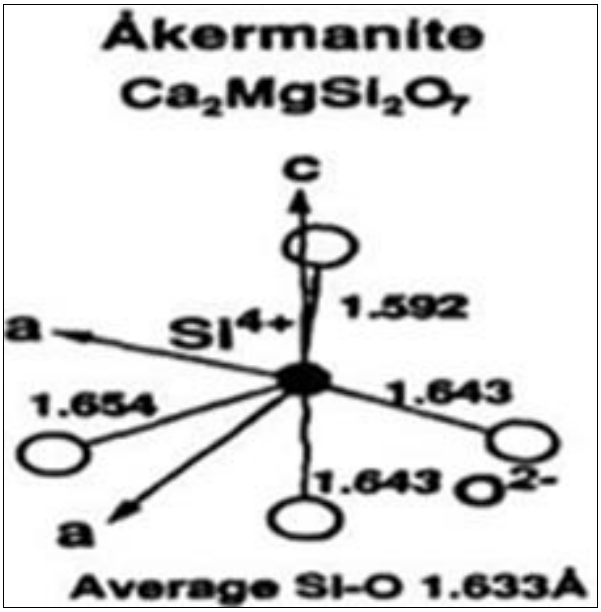

Fig 3: In CMS Crystal Structure, Inter-atomic Distance and Site Symmetry of Silicon Site

Table 2: The physical and chemical properties of CMS Phosphor

No.	Chemical Composition	Crystal Structure	Chemical Properties	Cations for substitution & their size	Coordination Number of the crystal lattice sites for substitution
1.	$Ca_2MgSi_2O_7$	Tetragonal Akermanite	Stable and Biocompatible	Mg^{2+} (0.72) Ca^{2+} (0.99)	Ca_1(1:6), Ca_2(2:8) Mg (4)

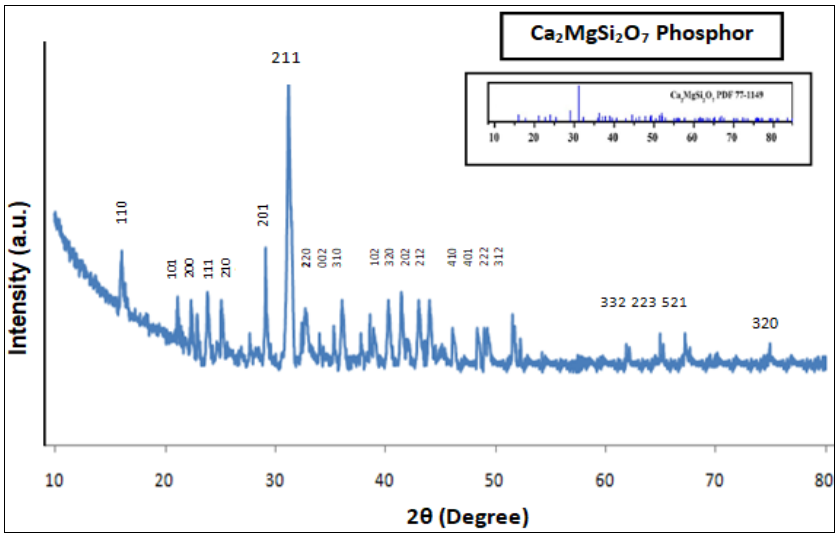

Fig 4: XRD Pattern of Un-doped CMS Sample

Usually, we completely agree that the oxidizers &fuel are compulsory required for any combustion synthesization technique. In this process, metal nitrates (i.e. as oxidizers) and urea (i.e. as fuel) are also employed. Based on propellant chemistry, it is very essential to calculate the stoichiometric molar-ratio of all metal nitrates; oxidizers and fuels are used in this experiment, so that the chemical reaction can be balanced [Ekamabaram *et al*. (2005)] [28]. With the calculation of oxidizer to fuel ratio, the elements were assigned formal valences as follows: Ca = +2, Mg = +2, Si= +4, B = +3, C = +4, H = +1, O = -2 and N = 0. For complete combustion process, it is very important that the oxidizer and fuel serve as a numerical-coefficient to maintain the stoichiometric equilibrium, so that the equivalence ratio is equal to unity (i.e. total oxidizing valency/total reducing valency (O/F) = 1), and the maximum energy is released [Kingsley *et al*. (1988)] [29].

Table 3: The elements were assigned formal valences

No.	Elements	Atomic Number (Z)	Electronic Configuration	Formal Valences
1.	Calcium (Ca)	20	2, 8, 8, 2	+2
2.	Magnesium (Mg)	12	2, 8, 2	+2
3.	Silicon (Si)	14	2, 8, 4	+4
4.	Boron (B)	5	2, 3	+3
5.	Carbon (C)	6	2, 4	+4
6.	Hydrogen (H)	1	1	+1
7.	Oxygen (O)	8	2, 6	-2
8.	Nitrogen (N)	7	2, 5	0

FESEM Analysis

The FESEM instruments also utilize a focused beam-ray of high-energy-electrons at the specimen-plane to originate various signals. In this way, signals obtained through the electron-sample protection displays sample information related to the external morphology, chemical composition and crystalline structure as well as configuration of the sample-creating material. The selected field with a range between (i.e. almost 1cm-5micron width) in a scanning mode utilizing morphological image can be done [Goldstein *et al*. (1981) [30], Egerton *et al*. (2005) [31], Williams *et al*. (1984)] [32]. SEM has also proven the virtue of being able to analyze of picked spot positions on a specimen. It is the most essential investigation of qualitative or semi-quantitative chemical compositions (i.e. utilize in EDS), crystalline phase structure and crystal assortments are dependent on its behavioral point of view [Clarke *et al*. (2002)] [3]. The luminescent property of any phosphor samples depends on particles morphology (i.e. shape, size, and its defects) [Reed *et al*. (2005)] [34]. In Fig: 5, the surface morphology (i.e. SEM Images) of the sintered CMS sample has shown with 200nm magnification. Thus, when the SEM images are investigated closely, the particles shapes are tightly interconnected in an irregular spherical form. The availability of agglomerate particles, voids and pores was ensured because of the gases released during the combustion process. During observation, it was also found that the phosphor sintered via combustion synthesis technique is less compact than the traditional solid-state reaction technique (i.e. high-temperature process).

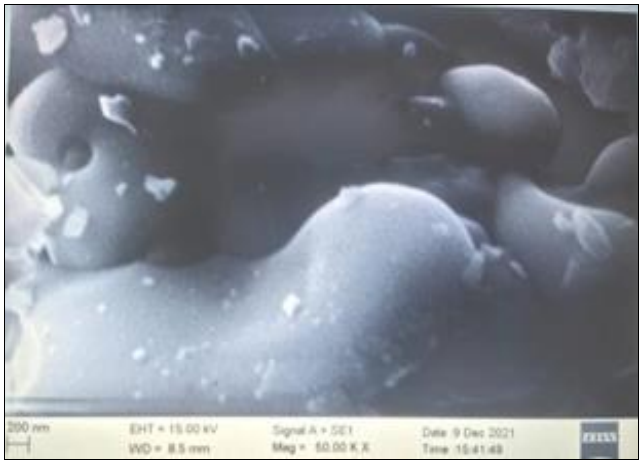

Fig 5: FESEM Image of $Ca_2MgSi_2O_7$ (CMS) Phosphor

Energy Dispersive X-Ray Spectroscopy (EDX)

Fundamentally, EDX analysis is demonstrated as EDS or EDAX that has been shown to be more beneficial as an X- ray analysis technique for identifying the elemental composition

of material samples. Its consumptions include such as substances and products research, refining, de-formulation and much more. The EDX system plays an important role of enclosure for electron microscopy instruments such as SEM (Scanning Electron Microscope) or TEM (Transmission Electron Microscope). In this way, both SEM & TEM instruments are complement to each other. Additionally, the imaging durability of the both microscope plays a specific role in the recognition of the specimen's interest [Goldstein *et al*. (1981) [30], William *et al*. (1984)] [32]. In order to better quantify & identify properties of the elemental components or chemical characterization of the any specimen spotting area. This technique is put to practical use, which is as small as nanometers (nm) range. The data achieved through EDX analysis clearly shows the presence of spectral peaks. Under this study, the spectral peak is obtained resembling the elements that make up the actual composition of the sample [Goldstein *et al*. (1981)] [30]. Fig: 6 show the EDX spectrum of sintered $Ca_2MgSi_2O_7$ phosphor sample. From the analysis of spectrum it is found that the emission peaks of Calcium (Ca), Magnesium Mg & Silicon Si as well as Oxygen O compositional elements are clearly evident in this spectrum. In the meantime, they do not reveal any emission peaks of any kind. The presence of an intense emission peak displays that this is ensured by the actual structure formation of the phosphor sintered through the combustion synthesis route. Table: 4 represents that the elemental compositions of sintered CMS sample. In this way, they are compared with the ideal $Ca_2MgSi_2O_7$ (CMS) phosphor.

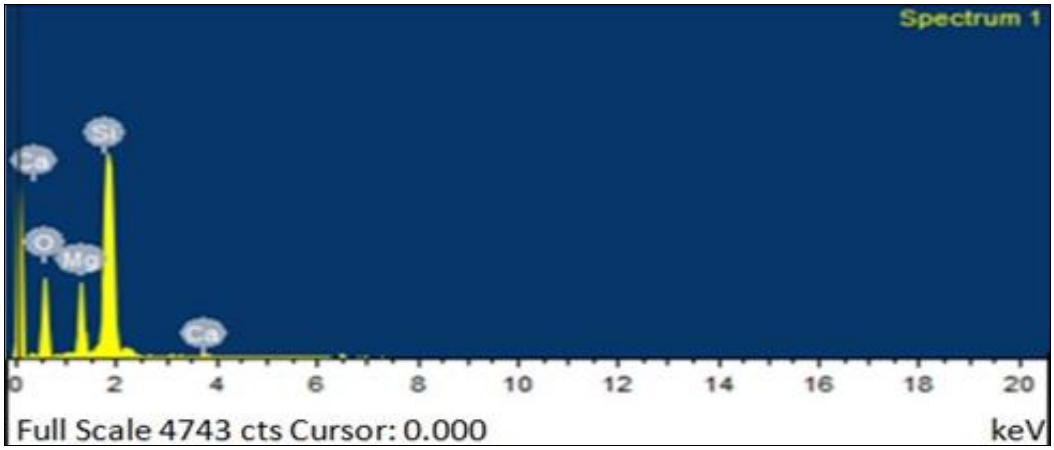

Fig 6: EDX Spectrum of sintered CMS Sample

Table 4: Elemental Composition of sintered CMS Sample

Elemental Composition			
No.	**Chemical Elements**	**Atomic (%)**	**Weight (%)**
1.	O K	48.84	65.38
2.	Mg K	6.14	5.90
3.	Si K	16.64	13.18
4.	Ca L	28.38	15.54
Total		100.00	100.00

Fourier Transform Infra-Red Spectroscopy (FTIR)

This spectroscopic technique is the most significant and useful technique, which is utilized to recognition and determine the absorption band of the various functional groups of any chemical compound. Its special properties can also be used to obtain knowledge about certain components of an unnamed mixture. During observation of a chemical compound, it also exhibits IR radiation as well as vibrational motion [Makreski *et al*. (2007) [35], Stuart *et al*. (2004)] [36]. In this present work, determination of all absorption bands and functional groups were determined between in the range of (4000 - 400 cm^{-1}) [Nakamoto *et al*. (2009)] [38] under FTIR spectra. Recently, computerized FTIR devices are better utilized. Thus, they prove to be faster and more sensitive powerful tools than the old-fashioned dispersive devices [Kauppinen *et al*. (2001)] [37]. The sintered CMS phosphor FTIR spectrum has been displayed in Fig: 7. At 961.27cm^{-1}, an intense band are situated which is responsible due to the evidence of (Si-O-Si) asymmetric stretch. The band at 871.72 cm^{-1} is located due to the (Si-O) symmetric stretch. At 597.62 cm^{-1} and 486.61cm^{-1}, bands are situated because of the presence of (Si-O-Si) group in vibrational mode. In addition, the absorption bands can be amenable to the clearly evidence of silicate (SiO_4) group [i.e. at 688.34 cm^{-1} and 1364.28 cm^{-1}] [Gou *et al*. (2005)] [39]. At 1866.39cm^{-1}, the band is situated due to the existence of small amount of the calcite. At 1866.39 cm^{-1}, the spectrum band is situated due to the existence of asymmetry stretching of carbonate $(CO_3)^{2-}$ functional group which have recorded in the range between (1900−1700cm^{-1}) [Vicentini *et al*. (2000)] [40]. At 1671.53 cm^{-1}, the band can be responsible due to the vibration of magnesium [Mg^{2+}] ions. Likewise bending of sharp peaks have situated (i.e. at 871.72cm^{-1}, 778.15cm^{-1}, and 745.12 cm^{-1}) which are amenable due to the stretching vibration of Ca^{2+} ions [Chandrappa *et al*. (1999) [41], Frost *et al*. (2007) [42], Salim *et al*. (2009)] [43]. At 3467.74 cm^{-1}, the band is centered due to the existence of stretching vibration of (O-H) hydroxyl functional group. It is clearly indicate that the evidence of (O-H) hydroxyl group due to moisture of this sample. The clearly evidence of (Mg-O) group due to the spectral band is situated at 486.61 cm^{-1} [Salim *et al*. (2009) [43], Caracas *et al*. (2003) [44], Sharma *et al*. (2021)] [45].

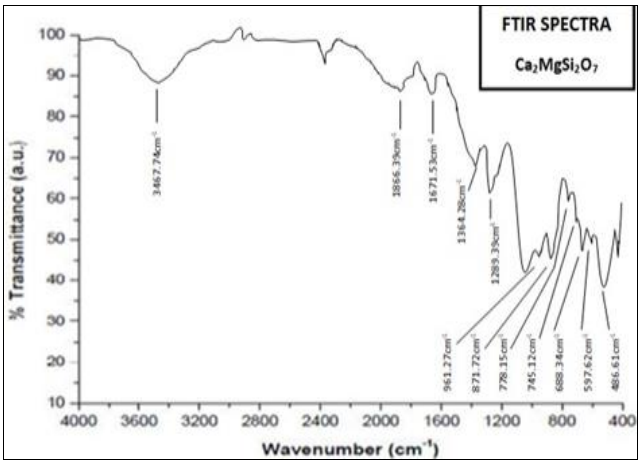

Fig 7: FTIR Spectra of Sintered CMS Sample

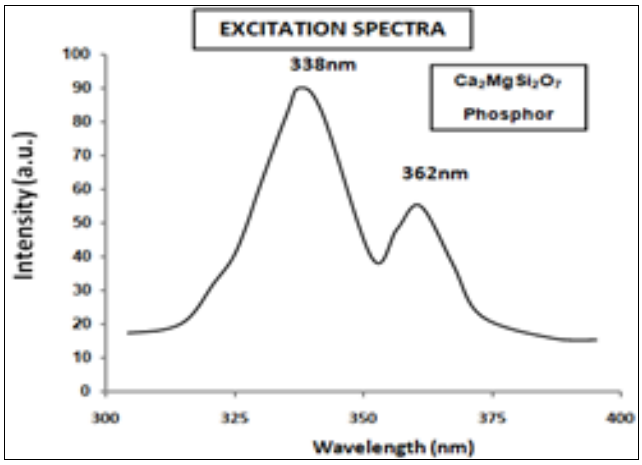

Fig 8: (a) Excitation Spectra of CMS Phosphor

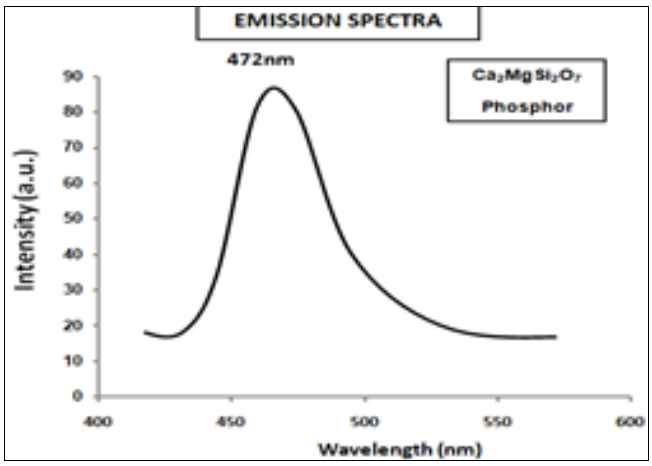

Fig 8: (b) Excitation Spectra of CMS Phosphor

Photoluminescence (PL) analysis

The phenomenon of PL (i.e. cold light source) is a just opposite process of Incandescence (i.e. hot light source). In simple words, an exclusive kind of luminescence produced during the process of light being emitted due to the absorption of photon particles which is called photoluminescence. Compared to the other optical characterization processes (i.e. reflection and absorption), the process of PL exhibits the phenomenon of being less stringent regarding beam-alignment, sample-thickness and surface-flatness. Analyzing the exclusive advantages of PL characteristics is revealed during the analysis, which is widely examined from the naivety of optical-mensuration and power to investigate compulsory for electronic merits [Ozawa *et al*. (2018)] [46]. These alkaline earth (AEs) metals [i.e. Sr (Strontium) & Ca (Calcium) as well as Ba(Barium)] rare-earth doped silicates have also been broadly studied as long after-glow luminescence-materials (i.e. phosphors), because of a new growing market for their wide range of application in traffic signs, decoration and textile printing, among others. Compared to previously utilized the sulphide phosphors (i.e. luminescent materials), silicate phosphors exhibits superior features likewise longer and brighter luminescence emission, facile and very low-cost (i.e. cheaper) as well as rapid synthesization of materials [Chandra *et al*. (2013) [47], Chen *et al*. (2009) [48], Chandrakar *et al*. (2015) [49], Chang *et al*. (2005)] [50].

The PL analysis of pure CMS sample has been studied based on the excitation and emission spectra [i.e. Fig. 8(a) & 8(b)]. Analysis of excitation spectra clearly shows that the spectral lines are found [i.e. at 300-400 nm wave length].At 338nm wave length, the optimum peak is centered and some-other spectral peak at 362nm. Simultaneously, the major peak allocated in blue color region at 472nm emission wave length [i.e. (400-600nm)]. Based on the PL analysis, we can say that both excitation and emission spectra of pure CMS Sample are displayed on very-low intensity [Sharma *et al*. (2021)] [9].

CIE color chromaticity diagram

Colour coordinates are the most significant factors for estimating phosphors performance. To calculate the phosphor performance on colour of luminescent emission spectra, Commission International de I'Eclairage (CIE) chromaticity co-ordinates were calculated adopting standard procedures. The luminescent-color is the most essential and important factor for application of phosphors (i.e. luminescent materials). In this way, the color emission of any phosphors (i.e. luminescent materials) are also examined and well elucidated with the help of chromaticity colour coordinates (i.e. CIE diagram) [CIE (1931) [51], CIE Color Spaces-SPIE books]. This colour coordinate of phosphors were examined based on a clear observation of their emission spectra. The CIE diagram of un-doped CMS phosphor is clearly displayed in Fig: 9. It is very clear from the calculated colour-chromaticity coordinate that this [X = 0.2445, Y = 0.2679] co-ordinate represents the blue light emission from the phosphor. As a result, the colour chromaticity co-ordinate of the luminescent-color emission has been displayed by this phosphor, approaches very close to blue light colour region.

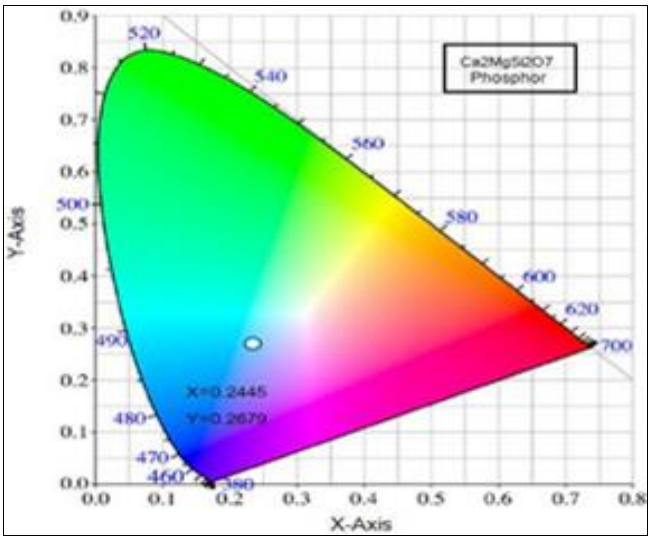

Fig 9: CIE Diagram of CMS Phosphor

Thermo luminescence [TL] Study

The TL analysis is well introduced as the occurrence of radiation emission process upon heating of a solid-sample material, that is, after the preceding energy-absorption i.e. during the irradiation process. In this way, we have assigned the general meaning of TL, that the heating procedure itself is the primary energy origin of the luminescence. Precise investigations suggest that this phenomenon is not in actually true, as it is quite discontinuous from the radiation involuntarily released from a material sample. For this reason, when it is heated to incandescent (i.e. hot source) [Murthy *et al*. (2008) [52], McKeever *et al*. (1985)] [53]. Based on experimental analysis, it has often been found that the thermo-luminescence [TL] materials exhibit afterglow properties, which is called as persistent luminescence. As a result, they are very strongly useful in various applications such as glow in the darkness road and emergency sign as well as bio-imaging fields [Luo *et al*. (2015)] [54]. In recent years, the rapid evolution of novel phosphor materials has been examined. The main reason behind this is to demonstrate a new and rapidly emerging application of research in the fields of physics, medicine area (i.e. medical treatment) as well as archaeological dating, forensic science radiation dosimetry and mineral prospering areas etc. which are continuously being explored [Pratibha *et al*. (2014) [55], Rivera *et al*. (2011)] [56].

Evaluation of Trapping Parameters

The silicate materials can be considered as photo-luminescent or thermo-luminescent due to their nature of energy storage and which generate luminescence by either photo or thermo-stimulation [Mckeever *et al*. (2011) [57], Bas AJ *et al*. (2006) [58]]. Thus, among the various silicates the selection of the proper host and activators is an important issue for TL. The combination of host, do-pant and the optimum doping percentage of do-pants plays the significant role for creating luminescence centers and helps in making sensitive TL phosphors. TL luminescent-materials (i.e. phosphors) demonstrate glow-curve peaks with one or more peaks. In such a case, when the charge carriers (i.e. holes or electrons) are freed. When TL analysis of any phosphor, then the TL glow-curve of that phosphor primly depends on the kinetic (i.e. trapping) parameters which mainly comprise such as [Order of Kinetics b] and [Frequency Factor s^{-1}] as well as [Activation Energy E or Trap Depth] [DR Vij (1998) [64]].

There are different methods which are applied for examining the kinetic parameters (i.e. trapping parameters) from thermo-Luminescence [TL] glow curve peaks. For instance, the TL glow-curve peak appears to be highly isolated from each other's. The most popular experimental method is known as peak shape method. The peak shape method is well appropriate method for the determination of kinetic parameters (i.e. trapping parameters). These parameters were analyzed for the optimal TL glow-curve peak of sintered phosphor samples with the help of this method [Shrinivas *et al*. (2012) [59].

Peak Shape Method

To determine the trapping parameters the peak shape method is being used. The temperature at different points of the glow peak has been used to calculate the parameters using the given formula. Peak shape method [Fig: 10] is an analytical technique which was proposed by Chens, thus also known as Chen's method [Shrinivas *et al*. (2012) [59]]. This method is also useful to detect the position of energy levels in the forbidden energy gap and defect centers [Pagonis *et al*. (2006)] [60]. Therefore, the complete analysis of glow curve has been done using this method. Fig: 10 shows that the peak shapes of glow curve of the prepared sample. T_m, T_1 and T_2 are maximum, lower (ascending part of glow curve) and higher (descending part of glow curve) temperature at half the intensity, respectively [Ekdal *et al*. (2007) [61], Jose *et al*. (2011)] [62], and other kinetic parameters (τ, δ, ω) are originated using these temperatures, where Tm-T_1 defines τ, T_2-T_m gives δ and T_2-T_1 defines ω. Using these parameters activation energy, order of kinetics and frequency factor is evaluated.

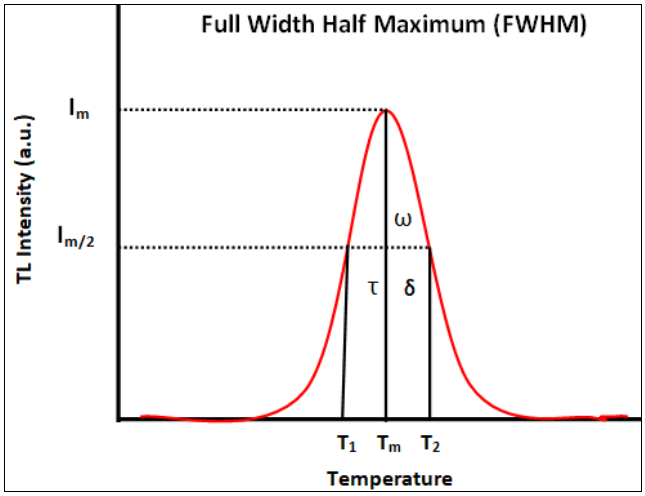

Fig 10: Peak Shape FWHM Method

Order of Kinetics (b)

This kinetic parameter is clearly displays the dependence on the peak shape of TL glow-curve. It is clear to say that the mechanism of recombination process of de-trapped charge-carriers (i.e. electrons or holes) with their samples is called order of kinetics [b]. For glow-curve peak, this parameter can be evaluated with the help of shape factor (i.e. geometric factor) μ_g determination from the following mathematical form as below.

$$\mu_g = \delta/\omega = T_2 - T_m/T_2 - T_1 \quad (2)$$

Where T_m represents the prominent peak temperature and T_1

& T_2 are represents temperatures at half intensity on the ascending and descending orders of the glow-curve peak, respectively and $\omega = T_2 - T_1$ and [$\delta = T_2 - T_m$]are represents the high-temperature half-width. The geometric shape factor is key part of TL glow-curve peak which is to differentiate between 1st and IInd order kinetics. The mathematical value of geometric factor [μ_g = 0.39-0.42] represents for the 1st order kinetics and [μ_g = 0.49−0.52] represents for the 2nd order kinetics as well as for the mixed order kinetics also represent as [μ_g = 0.43-0.48] [Pagonis *et al*. (2006) [60], Ekdal *et al*. (2007) [61], Jose *et al*. (2011) [62], Deshpande *et al*. (2016)] [63].

Activation Energy (E) or (Trap Depth)

The trapped electron needs some amount of energy to free itself, also known as activation energy (i.e. trap depth)which is required to liberate an electron to the conduction band from defects center [Pratibha *et al*. (2014)] [55]. The value of trap-depth (i.e. activation energy) can be evaluated with the help of the following mathematical equation as mentioned, which is valid for any kinetics (i.e. first, second and mixed order kinetics).

$$E = C_\alpha \left(\frac{kT_m^2}{\alpha}\right) - b_\alpha (2kT_m) \quad (3)$$

Cα and bα (where α = τ, δ, ω) are determined with the help of the following mathematical equation, which is valid for any general order kinetics [Sharma *et al*. (2018)] [65]:

$C_\tau = 1.51 + 3\ \mu_g - 0.42]$, $b_\tau = [1.58 + 4.2(\mu_g - 0.42)$ (3.1)

$C_\delta = 0.976 + 7.3\ \mu_g - 0.42$, $b_\delta = 0$ (3.2)

$C_\omega = 2.52 + 10.2\ \mu g - 0.42$, $b_\omega = 1.0$ (3.3)

Frequency Factor (s^{-1})

The occurrence of this trapping parameter are clearly indicates the probability of an electron escaping from the traps after exposure to ultra-violet (i.e. UV) radiation. This kinetic parameter is one of the most significant parameters which are used for sample characterization process [Deshpande *et al*. (2016)] [63]. This trapping - parameter is calculated by substituting the previously evaluated values of order of kinetics [b] and activation energy E in the mathematical equation (as mentioned):

$$\frac{\beta E}{kT_m^2} = s\left[1 + (b-1)\frac{2kT_m}{E}\right]\exp\left(-\frac{E}{kT_m}\right) \quad (4)$$

Where k represents Boltzmann constant, E represents activation energy & b represents an order of kinetics, T_m represents the prominent temperature of glow-curve peak position, and β (i.e. at present work 5^oCs^{-1}) represents the heating rate of the any material sample [Pagonis *et al*. (2006) [60], Ekdal *et al*. (2007) [61], Jose *et al*. (2011)] [62].

The TL glow-curve peak of sintered CMS sample has been displayed in Fig: 11. In has been found in the analysis that the glow-curve peak was centered at 152.43°C temperature with 15 min UV-irradiation time at 5^oCs^{-1} constant heating rate. This peak of the sample is very weak which are found in our case and it can be neglected. Observing the TL glow curve, we find that the maximum glow curve is obtained at 152.43°C temperature, respectively. From 38.18°C temperature, TL intensity is continuously increasing up to 152.43°C, respectively. There after that the TL intensity is decreasing continuously up to 230.31°C and their after TL intensity curve is near about flate and constant having the lowest value of TL intensity up to 300°C

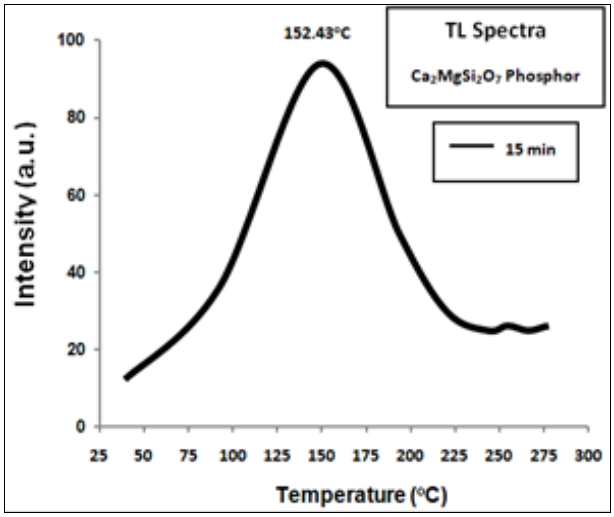

Fig 11: TL glow-curve peak of CMS sample

Table 5: The kinetic parameters of sintered CMS sample

Trapping Parameters										
UV min	HTR	T_1 (°C)	Tm (°C)	T_2 (°C)	τ	δ	ω	$\mu_g = \delta/\omega$	E (eV)	Frequency factor s^{-1}
15	5^oCs^{-1}	107.63	152.43	202.66	44.80	50.23	95.03	0.53	0.50	5.6 X 10^7

The effect of 15 min UV exposures time on the un-doped $Ca_2MgSi_2O_7$ (CMS) sample and different thermo-luminescence [TL] kinetic (i.e. trapping) parameters such as [activation energy (i.e. trap depth) (E), and frequency factor (s^{-1}) as well as order of kinetics (b)] are evaluated in Table: 5. The Geometric shape factor (μ_g) is calculated as 0.53, which indicates second order kinetics. Along with this, corresponding evaluated value of activation energy (E) is 0.50 eV and frequency factor (s^{-1}) has been obtained as 5.6×10^7 s^{-1}.

Applications of future scopes

Akermanite earth silicates have been broadly studied as host materials for phosphor application because of their chemical and physical stability and varied luminescent color. Thus, the material is a suitable host for phosphor application in white light emitting diodes (WLEDs) and solid-state lighting (SSL) devices. Compared to sulfide phosphors, silicates phosphors play an important contribution among many inorganic phosphors. The most significant factor behind all this is the fact that they possess vast chemical and structural variations. Usually, they have large band gaps as a host matrix. Presently, this phosphor has been widely utilized prominently in specific beneficial areas likewise Cancer-Therapy, Drug-delivery, Bone-Materials, Bone-Tissue Engineering, Bio-Materials and Tissue Engineering applications. Along with

this, it is also making its significant contribution in the field of DNA transplantation technique in medical science and computer application (i.e. for Image Processing) as well as operation research, Information technology areas.

Conclusion

The host $Ca_2MgSi_2O_7$ (CMS) nano phosphor was successfully synthesized via combustion synthesis technique. The analysis of XRD patterns reveals the formation of single-phase tetragonal/Akermanite crystal structure. FESEM images displays that this phosphor is comprised of irregular pores with the nano crystal structure composition of slight particles very close to the pores. The pores are approximately disordered (i.e. unarranged). The elemental composition of sintered phosphor was compared with the standard element with the help of EDS spectra. The silicate (SiO_4) absorption bands and different functional groups of related pure compound to well agreement for actual clarifications have been investigated under the FTIR spectra. At 472nm emission wavelength, the major peak Located in blue light region. On the basis of comparison of PL results, we can say that the host CMS phosphor has been shown both excitation and emission spectra at comparatively very low PL intensities. The CIE chromaticity diagram of the sintered phosphor are carried out and reached to blue luminescence color emission respectively. The TL glow curve peak was allocated at 152.43°C temperature respectively, and this peak position remains constant with 15min UV irradiation time. In our case, the TL glow curve peak is very weak with non-systematic and it can be neglected. After this overall study, it would be fair to say that the PL & TL intensities do not achieve their optimum level due to the large band gap in the host materials. This is the reason why doping process should be adopted to narrow band gap so that PL & TL glow curves can be obtained at higher intensities.

Acknowledgement

Authors are also thankful to Dr. G.S. Sao, Dept. of Mathematics, Govt. E. R. R. P.G. Science College Bilaspur (C.G.). He helps to us for Mathematical calculation of TL parameters. We are obliged the kind support Dept. of Metallurgical Engineering & Dept. of physics, NIT Raipur (C.G.)for the facility of XRD, SEM & FTIR analysis and Dept of physics, Pt. Ravishankar Shukla University, Raipur (C.G.) India for conferring us the facility of TL and PL analysis. We are also most heartily thankful to Dept. of Physics, Dr. Radha Bai, Govt. Navin Girls College Mathpara Raipur (C.G.), conferring us the accommodation of muffle furnace and other required research instruments.

Conflict Of Interest

The authors have not received any financial support for the research work, authorship and publication of this article.

References

1. Matsuzawa T, Aoki Y, Takeuchi N, Murayama Y. A new long phosphorescent phosphor with high brightness, $SrAl_2O_4$: Eu^{2+}, Dy^{3+}. Journal of the Electrochemical Society. 1996;143(8):2670.
2. Tam TTH, Du NV, Kien NDT, Thang CX, Cuong ND, Huy PT, *et al*. Co-precipitation synthesis and optical properties of green-emitting $Ba_2MgSi_2O_7$:Eu^{2+} phosphor. Journal of luminescence. 2014;147:358-362.
3. Tingqiao LEOW, Hong LIU, Hussin R, Ibrahim Z, Deraman K, Lintang HO, *et al*. Effects of Eu^{3+} and Dy^{3+} doping or co-doping on optical and structural properties of $BaB_2Si_2O_8$ phosphor for white LED applications. Journal of Rare Earths. 2016;34(1):21-29.
4. Yuan B, Huang Y, Yu YM, Seo HJ. Luminescence and structure of Eu^{2+}-doped $Ba_2CaMg_2Si6O1_7$. Ceramics International. 2012;38(3):2219-2223.
5. Ju H, Wang B, Ma Y, Chen S, Wang H, Yang S. Preparation and luminescence properties of $Na_4CaSi_3O_9$: Ce^{3+} phosphors for solid state lighting. Ceramics International. 2014;40(7):11085-11088.
6. Liu S, Liang Y, Zhu Y, Wu X, Xu R, Tong M, *et al*. Synthesis and luminescence properties of novel Ce^{3+} doped $BaZrSi_3O_9$ phosphors. Optics & Laser Technology. 2016;84:1-8.
7. Tshabalala MA, Swart HC, Dejene FB, Coetsee E, Ntwaeaborwa OM. Structure, surface analysis, photo luminescent properties and decay characteristics of Tb^{3+}-Eu^{3+} co-activated $Sr_2MgSi_2O_7$ phosphor. Applied Surface Science. 2016;360:409-418.
8. Bhatkar VB, Bhatkar NV. Combustion synthesis and photoluminescence study of silicate biomaterials. Bulletin of Materials Science, 2011;34(6):1281-1284.
9. Sharma S, Dubey SK. The Significant Properties of Silicate Based Luminescent Nano materials in Various Fields of Applications, A Review. International Journal of Scientific Research in Physics and Applied Sciences. 2021;9(4):37-41.
10. Karacaoglu E, Karasu B. Effect of activators and calcination on luminescence properties of åkermanite type phosphors. Indian Journal of Chemistry. 2015;54:1394-1401.
11. Sharma S, Dubey SK, Diwakar AK, Pandey S. Structural Characterization and Luminescence Properties of $Ca_2MgSi_2O_7$ (CMS) Phosphor. International Journal of Scientific Research in Physics and Applied Sciences. 2021;9(6):49-53.
12. Patil KC, Aruna ST, Mimani T. Combustion synthesis: an update. Current opinion in solid state and materials science. 2002;6(6):507-512.
13. Aruna ST, Mukasyan AS. Combustion synthesis and nano materials. Current opinion in solid state and materials science. 2008;12(3-4):44-50.
14. Patil KC, Hegde MS, Rattan T, Aruna ST. Chemistry of Nanocrystalline Oxide Materials: Combustion Synthesis, Properties and Applications; c2008.
15. Muresan L, Popovici EJ, Indrea E. Structural and luminescence characterization of yttrium oxide- based phosphors prepared by wet-chemical method. Journal of Optoelectronics and Advanced Materials. 2011;13(3):183.
16. Kim H. Atomic layer deposition of metal and nitride thin films: Current research efforts and applications for semiconductor device processing. Journal of Vacuum Science & Technology B: Microelectronics and Nanometer Structures Processing, Measurement, and Phenomena. 2003;21(6):2231-2261.
17. Friedbacher G, Bubert H. (Eds.). Surface and Thin Film Analysis: A Compendium of Principles, Instrumentation, and Applications. John Wiley & Sons; c2011.
18. Lyman CE, Newbury DE, Goldstein JI, Williams DB, Romig AD, Armstrong JT, *et al*. Scanning electron microscopy, X-ray microanalysis and analytical electron microscopy. Journal of the Electrochemical Society of India. 1993;42(4):262-263.
19. JCPDS PDF File No. 17-1149, JCPDS International

Center for Diffraction Data. American Mineralogist Crystal Structure Data-Base-Code AMCSD 0008032.
20. Sharma S, Dubey SK, Pandey S, Diwakar AK. Optical Characteristics of Novel WLED ($Ca_2MgSi_2O_7$: Dy^{3+}) Phosphor. North Asian International Research Journal Of sciences, Engineering & I.T. 2021;7(11).
21. Feitosa AV, Miranda MAR, Sasaki JM, Araujo-Silva MA. A new route for preparing CdS thin films by chemical bath deposition using EDTA as ligand. Brazilian Journal of Physics. 2004;34(2B):656-658.
22. Ubale AU, Sangawar VS, Kulkarni DK. Size dependent optical characteristics of chemically deposited nanostructured ZnS thin films. Bulletin of Materials Science. 2007;30(2):147-151.
23. Yao GQ, Lin JH, Zhang L, Lu GX, Gong ML, Su MZ. Luminescent properties of Ba $Ba_2MgSi_2O_7$: Eu^{2+}, Mn^{2+}. Journal of Materials Chemistry. 1998;8(3):585-588.
24. Lin JH, Lu GX, Du J, Su MZ, Loong CK, Richardson JW. J Phys. Chem. Solids. 1999;60:975-983.
25. Chaplot SL, Choudhury N. Phase transitions of enstatite $MgSiO_3$: A molecular dynamics study. Solid state communications. 2000;116(11):599-603.
26. Jung KY, Han KH, Jung HK. J Electro chem. Soc. 2009;156:J129-J133.
27. Yonesaki Yoshinori, Takahiro Takei, Nobuhiro Kumada, and Nobukazu Kinomura. Crystal structure of Eu^{2+}-doped $M_3MgSi_2O_8$ (M: Ba, Sr, Ca) compounds and their emission properties. Journal of Solid-State Chemistry. 2009;182(3):547-554.
28. Ekambaram S, Maaza M. Combustion synthesis and luminescent properties of Eu^{3+}-activated cheap red phosphors. Journal of alloys and compounds. 2005;395(1-2):132-134.
29. Kingsley JJ, Patil KC. A novel combustion process for the synthesis of fine particle α-alumina and related oxide materials. Materials letters. 1988;6(11-12):427-432.
30. Goldstein JI, Newbury DE, Echlin P, Joy DC, Fiori C, Lifshin E. X-ray spectral measurement: WDS and EDS. In Scanning Electron Microscopy and X-Ray Microanalysis Springer, Boston, MA; c1981. p. 205-273.
31. Egerton RF. Physical principles of electron microscopy. New York: Springer. 2005, 56.
32. Williams DB. Practical Analytical Electron Microscopy in Materials Science, Philips Electronic Instruments, Inc. Mahwah, NJ; c1984.
33. Clarke A, Eberhardt C, Eberhardt CN. Microscopy techniques for materials science. Wood head Publishing; c2002.
34. Reed SJB. Electron microprobe analysis and scanning electron microscopy in geology. Cambridge university press; c2005.
35. Makreski P, Jovanovski G, Kaitner B, Gajović A, Biljan T. Minerals from Macedonia: XVIII. Vibrational sectra of some sorosilicates. Vibrational Spectroscopy. 2007;44(1):162-170.
36. Stuart BH. Infrared spectroscopy: fundamentals and applications; 2004.
37. John Wiley, Sons Kauppinen J, Partanen J. Fourier transforms in spectroscopy. John Wiley & Sons; c2001.
38. Nakamoto K. Infrared and Raman spectra of inorganic and coordination compounds, part B: applications in coordination, organometallic, and bioinorganic chemistry. John Wiley & Sons; 2009.
39. Gou Z, Chang J, Zhai W. Preparation and characterization of novel bioactive dicalcium silicate ceramics. Journal of the European Ceramic Society. 2005;25(9):1507-1514.
40. Viceintini G, Zinner LB, Zukerman-Schpector J, Zinner K. Luminescence and structure of europium compounds. Coordination Chemistry Reviews. 2000;196(1):353-382.
41. Chandrappa GT, Ghosh S, Patil KC. Synthesis and Properties of Willemite, Zn_2SiO_4, and M^{2+}: Zn_2SiO_4 (M= Co and Ni). Journal of Materials Synthesis and Processing. 1999;7(5):273-279.
42. Frost RL, Bouzaid JM, Reddy BJ. Vibrational spectroscopy of the sorosilicate mineral hemimorphite $Zn_4(OH)_2Si_2O_7 \cdot H_2O$. Polyhedron. 2007;26(12):2405-2412.
43. Salim MA, Hussin R, Abdullah MS, Abdullah S, Alias NS, Fuzi SAA, *et al*. The local structure of phosphor material, $Sr_2MgSi_2O_7$ and $Sr_2MgSi_2O_7$: Eu^{2+} by infrared spectroscopy. Solid State Science and Technology. 2009;17(2):59-64.
44. Caracas R, Gonze X. Ab initio determination of the ground-state properties of $Ca_2MgSi_2O_7$ åkermanite. Physical Review B. 2003;68(18):184102.
45. Sharma S, Dubey SK, Pandey S, Diwakar AK. Structural Characterization and Luminescence Properties of $Ca_2MgSi_2O_7$ (CMS) Phosphor. International Journal of Research Publication and Reviews. 2021;2(11):321-326.
46. Ozawa L. Cathodoluminescence and photoluminescence: theories and practical applications. CRC Press; c2018.
47. Chandra BP, Chandra VK, Jha P. Models for intrinsic and extrinsic fracto- mechanoluminescence of solids. Journal of Luminescence. 2013;135:139-153.
48. Chen Y, Cheng X, Liu M, Qi Z, Shi C. Comparison Study of the Luminescent Properties of the white-light long afterglow phosphors: $Ca_xMgSi_2O_{5+x}$: Dy^{3+} (x= 1, 2, 3). Journal of luminescence. 2009;129(5):531-535.
49. Chandrakar P, Bisen DP, Baghel RN, Chandra BP. Synthesis and Optical Properties of $CaMgSi_2O_6$: Ce^{3+} Phosphors. Journal of Electronic Materials. 2015;44(10): 3450-3457.
50. Fei Q, Chang C, Mao D. Luminescent properties of $Sr_2Mg_Si2O_7$ and $Ca_2MgSi_2O_7$ long lasting phosphors activated by Eu^{2+}, Dy^{3+}. Journal of Alloys and Compounds. 2005;390(1-2):133-137.
51. CIE. International Commission on Illumination. Publication CIE no. 15 (E-1.3.1). CIE Color Spaces - SPIE Book, Digital Library; c1931. DOI: 10.1117/3.660835.ch5.
52. Murthy KVR, Reddy JN. Thermo-luminescence: Basic Theory, Applications and Experiments, Published by Nucleonix Systems Pvt. Ltd., Hyderabad, India; c2008.
53. McKeever SWS. Thermo-luminescence of Solids, Cambridge University Press. London New York; c1985.
54. Luo H, Bos AJ, Dobrowolska A, Dorenbos P. Low-temperature VUV photoluminescence and thermo luminescence of UV excited afterglow phosphor $Sr_3AlxSi_{1-x}O_5$: Ce^{3+}, Ln^{3+} (Ln= Er, Nd, Sm, Dy and Tm). Physical Chemistry Chemical Physics. 2015;17(23): 15419-15427.
55. Pratibha BS, Chandrashekara MS, Nagabhushana N, Ramesh KP, Nagabhushana BM. Chikka hanumanthrayappa, thermo luminescence studies on Sr2SiO4 nano powder. Procedia Mater Sci. 2014;5:944-52.
56. Rivera T. Synthesis and Thermo luminescent characterization of ceramics materials. Advances in Ceramics-Synthesis and Characterization, Processing and

Specific Applications; c2011.
57. McKeever SWS. Optically stimulated luminescence: a brief overview. Radiation Measurements. 2011;46(12):1336-1341.
58. Bos AJ. Theory of thermo luminescence. Radiation measurements. 2006;41:S45-S56.
59. Srinivas M, Rao BA. Luminescence studies of Eu^{3+} doped $BaGd_2O_4$ phosphor. Indian J Sci Technol. 2012;5(7):3022-6.
60. Pagonis V, Kitis G, Furetta C. Numerical and practical exercises in thermo luminescence. Springer Science & Business Media; c2006.
61. Ege AT, Ekdal E, Karali T, Can N. Determination of thermo luminescence kinetic parameters of $Li_2B_4O_7$: Cu, Ag, P. Radiation measurements. 2007;42(8):1280-1284.
62. Jose MT, Anishia SR, Annalakshmi O, Ramasamy V. Determination of thermo luminescence kinetic parameters of thulium doped lithium calcium borate. Radiation measurements. 2011;46(10):1026-1032.
63. Deshpande A, Dhoble NS, Gedam SC, Dhoble SJ. Photo and thermo luminescence in $K_2Mg(SO_4)_2$: Dy phosphor and evaluation of trapping parameters. Journal of Luminescence. 2016;180:58-63.
64. Vij DR. (Ed.). Luminescence of solids. Springer Science & Business Media; c2012.
65. Sharma M, Achuth PV, Deb D, Puthankattil SD, Acharya UR. An automated diagnosis of depression using three-channel bandwidth-duration localized wavelet filter bank with EEG signals. Cognitive Systems Research. 2018 Dec 1;52:508-20.